Calculations of Electronic Excitation Transfer: Applications to Ordered Phases in Polymeric Materials

L. Keller, D. M. Hussey, and M. D. Fayer*

Department of Chemistry, Stanford University, Stanford, California 94305

Received: December 11, 1995; In Final Form: March 29, 1996[⊗]

A general treatment of electronic excitation transfer (EET) for any random or nonrandom chromophore distribution is applied to finite-volume systems which can be modeled as spherical shells of finite thickness, cylinders, and lamellae. These geometries were chosen because they occur in a wide variety of materials of interest in synthetic polymer research, as well as in biological systems. The EET dynamics are described by the function $\langle G^s(t)\rangle$, the probability of finding the excitation on the originally excited chromophore. $\langle G^s(t)\rangle$ is directly related to the observables in fluorescence anisotropy and lifetime experiments, for donor−donor and donor−trap EET, respectively. The method is shown to be accurate in the limits for which analytical expressions in closed form are available. The model's usefulness in experimental design is demonstrated for the case of coronal swelling in spherical micelles of diblock copolymers. It was found that random labeling of the blocks which form coronae is the preferred method for observation of this effect and that the sensitivity can be enhanced by selectively tagging the junction of the two blocks with trap chromophores. The influence of the shape of the chromophore distribution function on $\langle G^s(t)\rangle$ was also investigated, to test the sensitivity of EET observables to the shape of the chromophore distribution at the A−B interface of a diblock copolymer material. The exact functional form of a symmetrical chromophore distribution was found not to appreciably affect the observables, while the spatial extent of the chromophore distribution has a major effect.

I. Introduction

In the polymer engineering industry and among academic scientists, there is tremendous interest in the structures of polymeric materials.[1] Industry often seeks to combine the characteristics of two different polymers by blending them, which results in an amazing repertoire of phase behaviors that affect the architecture and properties of the material. Diblock copolymers, whose blocks are each chemically identical with a different component of a blend, are often added to a blend in an effort to compatibilize its components and thereby stabilize the mixture. Materials containing or comprised entirely of diblock copolymers can order into starlike or brushlike spherical micelles, lamellae, disks, and cylinders of various sizes. These morphologies can be selected for by varying physical parameters such as block length, solvent characteristics, and blend temperature and composition. The relationships between these physical parameters and the phase behavior and molecular architecture of a polymeric material comprise a field that supports an exciting and quickly advancing frontier of scientific research.

Neutron scattering, transmission electron microscopy (TEM), and NMR techniques have revealed a great deal about polymer blend structure on a submicrometer scale, as is evident in reviews by Bates[1] and Schmidt-Rohr and Spiess.[2] These methods are most useful when the structures under investigation are abundant in the sample. Neutron scattering and TEM have the added requirement of high contrast between blend components, requiring large differences in their neutron scattering lengths or electron densities. NMR studies of ^{1}H spin diffusion are most closely related to optical studies of electronic excitation transport (EET), for which time-resolved observables are calculated in this work. Since the measurement of EET involves the detection of single photons against a dark background, EET experiments afford the unique sensitivity that permits probing the configurations of structures which are present in very low concentration and which contain very few chromophores.

The excited-state dynamics of systems of interacting chromophores are readily studied with fluorescence measurements. Fluorescent chromophores can transfer photoexcitations among themselves through nonradiative resonant dipolar interactions between excited and unexcited chromophores, as described by Förster.[3] The transfer interaction depends on the fluorescence−absorption spectral overlap between the excited singlet state of a donor and the ground state of an acceptor. This interaction is parametrized by the Förster distance, R_0, the distance at which the rate of transfer to unexcited chromophores is equal to the decay rate of the donor in the absence of acceptors. For chromophores in common use, R_0 ranges from 6 to 60 Å. Because Förster transfer is highly distance-dependent, dropping off as $(1/r)^6$, EET observables contain high-resolution information about chromophore spatial distribution. EET has been modeled such that a calculable quantity, $G^s(t)$, emerges, which is readily compared with experimental observables. $G^s(t)$ can also be calculated for triplet state excitation transfer or for photoinduced electron transfer using the procedures developed here, by substituting the appropriate form of the distance-dependent transfer rate for the Förster transfer rate, which is used explicitly here. Since the main emphasis of this work is to develop a theoretical base for the use of excitation transfer dynamics as a sensitive probe of polymer structure, the discussion is restricted to singlet states and Förster transfer. The distance dependence of Förster transfer is dependent on a single parameter, R_0, and R_0 can be determined spectroscopically. Triplet transfer and electron transfer, even when modeled in the simplest possible manner with a transfer rate that falls off exponentially with distance, are dependent on two parameters, and these parameters cannot be determined spectroscopically. Furthermore, it is straightforward to perform the necessary angle average for the Förster dipole−dipole transfer mechanism; it is not possible, in general, to perform the angle average for the triplet or electron

[⊗] Abstract published in *Advance ACS Abstracts,* May 1, 1996.

S0022-3654(95)03710-5 CCC: $12.00

transfer problems. Therefore, for the purposes of elucidating structure, Förster singlet excitation transfer dynamics are more useful.

The master equation for EET between randomly and nonrandomly distributed chromophores has a Green function solution which represents the density of excitations as a function of time and of the relative positions of chromophores.[4,5] $G^s(t)$ is the diagonal, or "self-" part of this Green function, which is the probability that an excitation is on an initially excited chromophore at time t, either because the excitation has not been transferred to another chromophore or because it has been transferred away from and returned to the initially excited chromophore. The observable arises from the distributions of unexcited chromophores around an ensemble of originally excited chromophores. Thus, the ensemble average of $G^s(t)$ is the quantity of interest. In a system containing a small number of donors and a large number of molecules that accept an excitation from a donor and do not pass it on (called a donor−trap, or DT, system), $\langle G^s(t)\rangle e^{-t/\tau}$ is simply equal to the donor fluorescence decay, where τ is the donor fluorescence lifetime in the absence of traps. In a system without traps, EET occurs among identical chromophores which will continually transfer excitations (called a donor−donor, or DD, system). In that case, the experimenter excites the chromophores with polarized light, such that those chromophores with a large projection of the light's $\vec{E}$ field along their absorption dipole are selectively excited. Excitation transport results in loss of polarization anisotropy of the ensemble of excited chromophores, and the observable is time-resolved fluorescence depolarization. Care must be taken to ensure that depolarizing processes other than EET, such as chromophore, copolymer, or micelle rotation, do not occur on the time scale of the experiment and that the orientational distribution of initially unexcited chromophores which will accept an excitation and subsequently fluoresce is not correlated with that of the photoselected ensemble. The time-dependent loss of fluorescence polarization anisotropy due to EET is then represented by $\langle G^s(t)\rangle$.[6]

Huber[7] developed a cumulant expansion method for calculating $\langle G^s(t)\rangle$ for EET among randomly distributed chromophores in an infinite volume. The expansion was truncated to first-order, such that only EET interactions between pairs of chromophores were considered. Peterson and Fayer[8] extended the theory to random distributions of chromophores in restricted geometries, including a finite spherical volume and a volume with the Gaussian morphology of a polymer chain, and Marcus and Fayer[9] treated the problem of calculating $\langle G^s(t)\rangle$ for EET between chromophores on a single sphere and on neighboring spheres. In this work we further develop the theory to apply to EET among chromophores in a random or any nonrandom distribution, in finite volumes having a wide range of shapes. The model is shown to behave exactly as predicted in those cases for which closed-form analytical expressions describing EET are available. A large body of literature is devoted to fluorescence experiments conducted to obtain high-resolution structural information about polymeric materials; however, models used to extract this information often rely on fitting data with exponential functions by adjusting parameters that do not represent physically meaningful quantities. To address the need for a model that allows straightforward interpretation of such data, and to explain which physical properties of a material must be measured along with the fluorescence observables to make meaningful interpretations, expressions and calculations of $\langle G^s(t)\rangle$ are presented for particular shapes that are currently of interest in the study of polymeric materials, *i.e.*, spherical shells of finite thickness, cylinders, and lamellae.

II. Theoretical Approach

The development of the method used for calculating $\langle G^s(t)\rangle$ has been described[7−10] as outlined above. Here, we discuss its extension to arbitrary chromophore distributions and to geometries that can be modeled as spherical shells and cylinders. Application of this theory to more complex morphologies is straightforward.

A. $\langle G^s(t)\rangle$ in a Spherical Shell of Finite Thickness. Moving from an expression for $\langle G^s(t)\rangle$ in infinite solution to expressions applicable to chromophores confined to finite volumes of various shapes entails losses of symmetry which must be accounted for explicitly. Therefore, $G^s(t)$ will vary with the location of the initially excited chromophore. $G^s(t)$ must be averaged over all possible locations of a second, unexcited chromophore about the initially excited chromophore and also over all possible locations of the initially excited chromophore. This double averaging is also necessary in an infinite solution with a nonrandom distribution of chromophores. The second consideration for finite volume systems is that there is a finite number of chromophores, so that the spatial average cannot be taken to the thermodynamic limit. The number of chromophores and the volume of the system must then be considered explicitly.

1. Donor−Donor Transfer. First, we express $\langle G^s(t)\rangle$ for an initially excited chromophore at a fixed point in space (denoted by subscript $i = 1$), averaging over all allowed positions of the chromophore that will accept its excitation (denoted by subscript $i = 2$):

$$\ln\langle G_1^S(t)\rangle = \frac{N-1}{2V_2}\int_{\mathbf{r}_2}(e^{-2\omega(r)t} - 1)u(\mathbf{r}_2)\,d\mathbf{r}_2 \qquad (2.1)$$

The integration is carried out over the space filled by the distribution of chromophore 2; $N - 1$ is the total number of chromophores 2, $u(\mathbf{r}_i)$ is a distribution function representing the spatial configuration of the chromophores, $V_2 = \int_{\mathbf{r}_2} u(\mathbf{r}_2)\,d\mathbf{r}_2$, and $\omega(r)$ is the rate of excitation transfer between two chromophores separated by the distance r (see section C). For a random distribution of chromophores, $u(\mathbf{r}_i) = 1$, and V_i is the total finite volume spanned by the chromophore distribution. In the spherical shell, the vector nature of the average is the equivalent of having a factor $4\pi r^2\,dr$ with the r a scalar. We then average over all allowed positions of chromophore 1:

$$\langle G^S(t)\rangle = (1/V_1)\int_{\mathbf{r}_1}\langle G_1^s(t)\rangle u(\mathbf{r}_1)\,d\mathbf{r}_1 \qquad (2.2)$$

with $V_1 = \int_{\mathbf{r}_1} u(\mathbf{r}_1)\,d\mathbf{r}_1$. The $u(\mathbf{r}_i)$ may take on any form.

For spherical symmetry, $u(\mathbf{r}) = u(r)$ with $r = |\mathbf{r}|$. For example, to describe a random chromophore distribution in a spherical shell of finite thickness, we use the step function

$$u(r) = \begin{cases} 1 & R_{in} \le r \le R_{out} \\ 0 & \text{otherwise} \end{cases} \qquad (2.3)$$

where R_{in} and R_{out} are the inner and outer radii of the shell, respectively. $\langle G^s(t)\rangle$ then has the form

$$\langle G^s(t)\rangle = \frac{3}{R_{out}^3 - R_{in}^3}\int_{R_{in}}^{R_{out}} \exp\left[\frac{3(N-1)}{4(R_{out}^3 - R_{in}^3)} \times \int_{R_{in}}^{R_{out}}\int_0^{\pi}(\exp[-2\omega(r)t] - 1)\, r_2^2 \sin\varphi\, d\varphi\, dr_2\right] r_1^2\, dr_1 \qquad (2.4)$$

The origin is at the center of the sphere; r_i is the distance from the origin to the position of chromophore i in the shell, and φ

is the angle between the vectors pointing from the origin to chromophores 1 and 2. The distance between the chromophores is then the length of the difference between these vectors:

$$r = \sqrt{r_1^2 + r_2^2 - 2r_1 r_2 \cos\varphi} \tag{2.5}$$

The experimental observable is time-resolved fluorescence depolarization.

2. Donor−Trap Transfer. For the simpler problem of describing EET in a DT system, in which one donor interacts with $N - 1$ traps, the master equation for $G^s(t)$ can be solved exactly. The average of $G^s(t)$ over the distributions of donor and trap chromophores[11,12] is

$$\langle G^s(t)\rangle = \frac{1}{V_1}\int_{\mathbf{r}_1} u(\mathbf{r}_1)\,\mathrm{d}\mathbf{r}_1\left[\frac{1}{V_2}\int_{\mathbf{r}_2} \mathrm{e}^{-\omega(r)t}\,u(\mathbf{r}_2)\,\mathrm{d}\mathbf{r}_2\right]^{N-1} \tag{2.6}$$

Again, as an example we use molecules randomly distributed in a spherical shell described in eq 2.4 and obtain:

$$\langle G^s(t)\rangle = \frac{3}{R_{out}^3 - R_{in}^3}\int_{R_{in}}^{R_{out}}\left[\frac{3}{2(R_{out}^3 - R_{in}^3)}\times \int_{R_{in}}^{R_{out}}\int_0^{\pi}(\mathrm{e}^{-\omega(r)t})r_2^2\sin\varphi\,\mathrm{d}\varphi\,\mathrm{d}r_2\right]^{N-1} r_1^2\,\mathrm{d}r_1 \tag{2.7}$$

The experimental observable is the decay of the donor fluorescence.

B. $\langle G^s(t)\rangle$ for Cylinders and Lamellae. So far, we have restricted our investigation to systems with spherical symmetry, but diblock copolymers order in a myriad of stable phases, depending on parameters such as block length or solvent characteristics. The application of this theory to symmetries other than the spherical is straightforward. After eqs 2.1 and 2.2 are written in cylindrical coordinates and simplifications due to the rotational symmetry of the cylinder are performed, $\langle G^s(t)\rangle$ for a DD system has the form

$$\ln\langle G_1^s(t)\rangle = \frac{N-1}{2V_2}\times \int_0^{2\pi}\int_{-L/2}^{L/2}\int_0^{R}(\mathrm{e}^{-2\omega(r)t} - 1)u(r_2)\nu(z_2)r_2\,\mathrm{d}r_2\,\mathrm{d}z_2\,\mathrm{d}\theta \tag{2.8a}$$

$$\langle G^s(t)\rangle = \frac{2\pi}{V_1}\int_{-L/2}^{L/2}\int_0^{R}\langle G_1^s(t)\rangle u(r_1)\nu(z_1)r_1\,\mathrm{d}r_1\,\mathrm{d}z_1 \tag{2.8b}$$

with $V_i = \int_0^{2\pi}\int_{-L/2}^{L/2}\int_0^{R}u(r_i)\nu(z_i)r_i\,\mathrm{d}r_i\,\mathrm{d}z_i\,\mathrm{d}\theta = 2\pi\int_0^{R}u(r_i)r_i\,\mathrm{d}r_i \times \int_{-L/2}^{L/2}\nu(z_i)\,\mathrm{d}z_i$. It is convenient to split the chromophore distribution function into a radial and a longitudinal part, reflecting the special symmetry of the cylinder. It is important that $u(r)$ and $\nu(z)$ may take on any form, as in the spherical model. $r = |\mathbf{R}_1 - \mathbf{R}_2|$ is the distance between donor and acceptor, with

$$\mathbf{R}_i = \begin{pmatrix} r_i\cos(\theta_i) \\ r_i\sin(\theta_i) \\ z_i \end{pmatrix} \tag{2.9}$$

Due to the rotational symmetry of the cylinder, we are allowed to introduce the relative angle θ between vectors pointing from the origin to chromophores 1 and 2, and r reduces to

$$r = \sqrt{r_1^2 + r_2^2 - 2r_1r_2\cos(\theta) + (z_1 - z_2)^2} \tag{2.10}$$

Equation 2.8b holds for disks and cylinders of any size. However, if the length of the cylinder is large compared with the length scale in EET experiments, that is, with the Förster distance R_0, we have translational symmetry along the cylinder axis, and eq 2.8b reduces to an expression for $\langle G^s(t)\rangle$ in an infinite cylinder:

$$\ln\langle G^s(t)\rangle = \frac{\rho}{2}\int_0^{2\pi}\int_{-\infty}^{\infty}\int_0^{R}(\mathrm{e}^{-2\omega(r)t} - 1)u(r_2)r_2\,\mathrm{d}r_2\,\mathrm{d}z\,\mathrm{d}\theta \tag{2.11a}$$

$$\langle G^s(t)\rangle = \frac{1}{A_1}\int_0^{R}\langle G_1^s(t)\rangle u(r_1)r_1\,\mathrm{d}r_1 \tag{2.11b}$$

Here $\gamma(z) = 1$, the distance $r = \sqrt{r_1^2 + r_2^2 - 2r_1r_2\cos(\theta) + z^2}$ and $A_1 = \int_0^{R}u(r_1)r_1\,\mathrm{d}r_1$.

Starting with eq 2.8b for a chromophore distribution with cylindrical symmetry, we are able to derive the expression for chromophores in lamellae or layers. Extending the limits of integration of r_1 and r_2 to infinity, we have translational symmetry in the plane perpendicular to the axis, and we obtain for $\langle G^s(t)\rangle$

$$\ln\langle G_1^s(t)\rangle = \pi\rho\int_{-L/2}^{L/2}\int_0^{\infty}(\mathrm{e}^{-2\omega(r)t} - 1)\nu(z_2)r_2\,\mathrm{d}r_2\,\mathrm{d}z_2 \tag{2.12a}$$

$$\langle G^s(t)\rangle = \frac{1}{\mathrm{H}_1}\int_{-L/2}^{L/2}\langle G_1^s(t)\rangle\nu(z_1)\,\mathrm{d}z_1 \tag{2.12b}$$

with $u(r) = 1$, $r = \sqrt{r_2^2 + (z_1 - z_2)^2}$, and $H_1 = \int_{-L/2}^{L/2}\nu(z_1))\,\mathrm{d}z_1$.

C. Rate of Electronic Excitation Transfer. The rate of excitation transfer between two chromophores separated by the distance r has been represented as $\omega(r)$. EET for singlet states also depends on the relative alignment of the chromophores between which an excitation is transferred. To take the orientation dependence of the EET into account, one writes the transfer rate as

$$\omega(r) = \frac{1}{\tau}\left[\frac{3}{2}\kappa^2(\Omega)\right]\left(\frac{R_0}{r}\right)^6 \tag{2.13}$$

where $\kappa^2(\Omega)$ is a unitless expression characterizing the interaction strength of a pair of dipoles as a function of their relative orientation.[13] If the relative orientations are dynamically averaged, $\omega(r)$ is averaged over the angular distribution of dipoles, $\nu(\Omega)$

$$\langle\kappa^2\rangle = \int_{\Omega}\kappa^2(\Omega)\nu(\Omega)\,\mathrm{d}\Omega \tag{2.14}$$

whereas in the static limit, $\langle G^s(t)\rangle$ as a whole must be averaged over this distribution.[12] Any $\nu(\Omega)$ may be included in this manner. In the dynamic limit with an isotropic angular distribution of dipoles, $\langle\kappa^2\rangle = 2/3$ and $\omega(r)$ reduces to

$$\omega(r) = \frac{1}{\tau}\left(\frac{R_0}{r}\right)^6 \tag{2.15}$$

Since for most systems involving polymers, the time scale for complete orientational randomization is long compared with the time scale for electronic excitation transfer, we work in the static limit. It has been shown[14] that in this limit the static transfer distance is obtained by multiplying the R_0 by the scaling factor $\gamma^{1/\Delta}$, with Δ the dimensionality of the system. Therefore, the average over angles only changes the effective R_0 of the system. The numerical value of γ depends on both the spatial dimension and the angular distribution $\nu(\Omega)$. For example, $\gamma = 0.8452$ for a three-dimensional system with an isotropic orientational distribution. Every R_0 used in the following calculations is a static transfer distance for randomly oriented chromophores.

III. Model Calculations

For several special geometries, analytical expressions in closed form for $\langle G^s(t)\rangle$ are available. A good test of the general

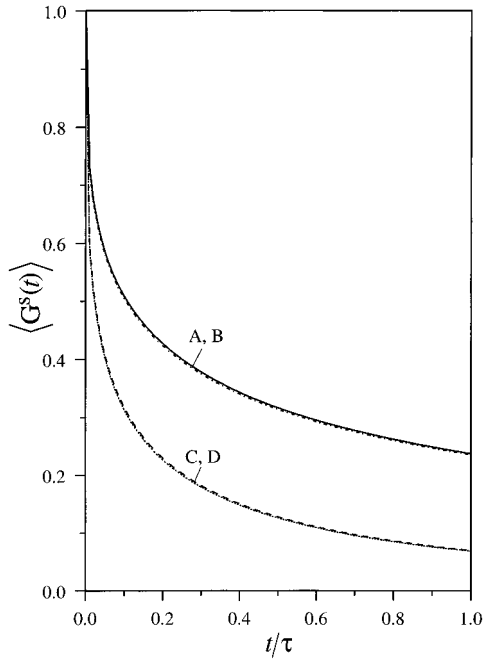

Figure 1. $\langle G^s(t) \rangle$ for donor−donor (curves A and B) and donor−trap (curves C and D) electronic excitation transfer for chromophores located on the surface of a spherical micelle. Curves A and C are calculated with the expressions for a spherical shell of finite thickness in the limit of zero thickness. Curves B and D use the closed-form expression for the surface of a sphere. In all cases, $N = 30$, $R_0 = 12.3$ Å, and the micelle radius is 14.0 Å.

model presented in this paper is the comparison of its behavior in limiting cases with these expressions.

In Figure 1 we compare the result of eq 2.4 in the limit of a sphere (an infinitely thin shell) with the analytical expression in closed form for DD EET on a spherical surface[9]

$$\langle G^s_{DD}(t) \rangle = \exp\left\{\frac{N-1}{2}\left[\mu_{DD}^{1/3}\gamma\left(\frac{2}{3}, \mu_{DD}\right) - \mu_{DD}^{1/3}\Gamma\left(\frac{2}{3}\right) + \exp(-\mu_{DD}) - 1\right]\right\} \quad (3.1)$$

which includes the complete and incomplete Euler gamma functions $\Gamma(a)$ and $\gamma(a, x)$, and

$$\mu_{DD} = 2\left(\frac{R_0}{2R}\right)^6 \frac{t}{\tau} \quad (3.2)$$

with R the radius of the sphere. Equation 2.4 was used with $R_{out} - R_{in} = 0.0001$ Å, so that the spherical shell was effectively reduced to a surface. The agreement between these expressions demonstrates the validity of eq 2.4 in this limit. Comparison of eq 2.7 with the analytical expression in closed form for DT EET on a sphere[12]

$$\langle G^s_{DT}(t) \rangle = \left[\mu_{DT}^{1/3}\gamma\left(\frac{2}{3}, \mu_{DT}\right) - \mu_{DT}^{1/3}\Gamma\left(\frac{2}{3}\right) + \exp(-\mu_{DT})\right]^{N-1} \quad (3.3)$$

where $\mu_{DT} = \mu_{DD}/2$ also results in exact agreement, as shown in Figure 1.

If the shell thickness remains negligibly small and the inner and outer radii are made to be very large with respect to R_0, the behavior of eqs 2.4 and 2.7 should be like that of $\langle G^s(t) \rangle$ for an infinite plane, for which the analytical expression in closed form is[14]

$$\ln\langle G^s_{2D}(t) \rangle = -\rho_{2D}\pi R_0^2 \lambda^{-2/3}\left(\frac{t}{\tau}\right)^{1/3}\Gamma\left(\frac{2}{3}\right) \quad (3.4)$$

in which ρ_{2D} is the area density of chromophores. Comparison of calculations of eqs 2.4 and 2.7 with eq 3.4 in both cases demonstrates that the general model behaves properly in this limit as well. It seems reasonable to expect eqs 2.4 and 2.7 to be applicable over the entire range of curvature and extension between the two limits studied here and in Figure 1.

The transition from sphere to plane with gradual increase of the sphere radius strongly depends on the chromophore density. Parts a and b of Figure 2 show examples of $\langle G^s(t) \rangle$ in DD systems for $C = 2$ and $C = 18$, with the reduced density $C = \rho 4\pi R_0^2$. In the higher density system, $\langle G^s(t) \rangle$ reaches the two-dimensional limit when the radius of the sphere is only $3R_0$, whereas low-density systems of the same size are clearly distinguishable from the two-dimensional limit. The limit for $C = 2$ is only reached when the sphere radius is more than $8R_0$.

Next, we examine the introduction of nonnegligible thickness by looking at the behavior of eq 2.4 for a fully filled spherical volume, *i.e.*, with $R_{in} = 0$. Although an analytical expression in closed form is not available, Peterson and Fayer[8] worked out this problem in detail for the DD case using the first-order cumulant approximation and showed that this expression was in very close agreement with more complete expressions for $\langle G^s(t) \rangle$. Their calculation involved a change of coordinates which moved the origin from the center of the sphere to the location of chromophore 1. We found that assigning the origin to the center of the volume enclosed by the shell made writing the more general expression tractable and faster to calculate. The results of both calculations are identical. We conclude that this model should hold for the entire range of shell thicknesses between the limits of a filled ball and a spherical surface.

When the geometry under consideration has cylindrical symmetry, we can examine the behavior of $\langle G^s(t) \rangle$ in two limiting cases. If the radial dimension of the cylinder is made very small with respect to R_0, the behavior of eq 2.8b should be like that of $\langle G^s(t) \rangle$ for a one-dimensional system, for which the analytical expression in closed form is[14]

$$\ln\langle G^s_{1D}(t) \rangle = -\rho_{1D} 2R_0 \lambda^{-5/6}\left(\frac{t}{\tau}\right)^{1/6}\Gamma\left(\frac{5}{6}\right) \quad (3.5)$$

Numerical evaluation of eq 2.8b in this limit showed excellent agreement with eq 3.5.

Equation 2.12b describes $\langle G^s(t) \rangle$ for a layer defined by $\nu(z)$. If the layer's thickness is very small compared to R_0, then eq 2.12b should behave like $\langle G^s(t) \rangle$ of an infinite plane. Numerical evaluation of eq 2.12b in this limit showed excellent agreement with eq 3.4.

We are now able to use the theory presented above to obtain a better understanding of the dependence of $\langle G^s(t) \rangle$ on the geometry of the system, which is important for planning and interpreting experiments. Consider a micelle of diblock copolymers with blocks A forming the core and the chromophore-bearing blocks B forming the corona. For simplicity, assume that the solvent does not appreciably penetrate block A, *i.e.*, the size of the core does not change. Changes in solvent properties, such as pH or ionic strength, or changes in temperature or pressure can lead to swelling or collapse of the shell (corona). Figure 3a shows calculations of $\langle G^s(t) \rangle$ in a DD system using eq 2.4 with a fixed inner radius and a fixed number of chromophores (30) in the shell. The swelling effect leads to dramatic changes in the decay of $\langle G^s(t) \rangle$. Even a rather small

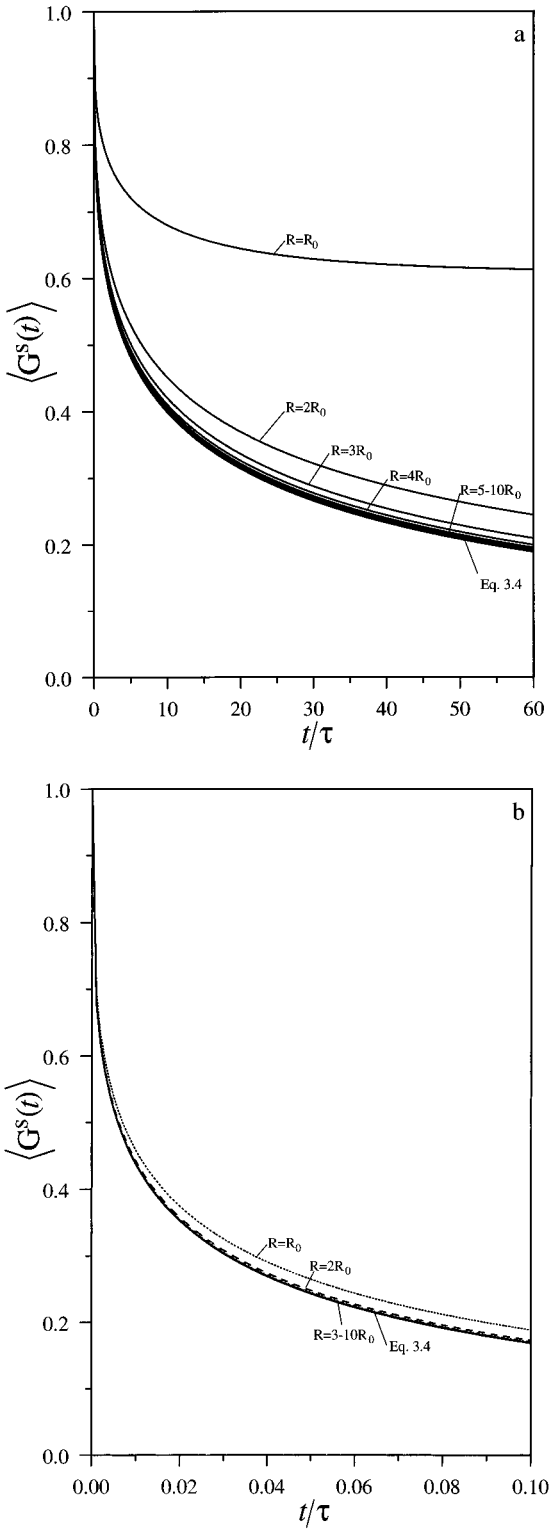

Figure 2. Approach of donor−donor $\langle G^s(t)\rangle$ in a zero thickness spherical shell to that in an infinite plane as the sphere radius (in units of R_0) increases, for (a) a low chromophore density ($C = 2$) and (b) a high density ($C = 18$), with the reduced area density $C = \rho 4\pi R_0^2$. The transition to the behavior of a plane occurs at smaller radii when the chromophore density is high. The difference between the decay curves decreases as the limit is approached; these curves in proximity to each other look like a single, thick line.

increase in the thickness of the shell leads to changes in the decay of $\langle G^s(t)\rangle$ which can be observed in fluorescence anisotropy measurements. Calculations for the same swelling process in a DT system are shown in Figure 3b. In the calculations, there is 1 donor and 29 traps. As expected, the decays are faster than the corresponding curves for the DD system, but the relative change of $\langle G^s(t)\rangle$, *i.e.*, the effect of the swelling itself on the observable, is comparable to that in the DD case. So far, we have used random distributions for donor and trap chromophores in the coronae. It is interesting to see the behavior of $\langle G^s(t)\rangle$ if either the donors or the traps are restricted to the inner boundary of the shell. This corresponds to diblock copolymer systems whose A−B junctions are labeled with donors (or traps), while the traps (or donors) are randomly distributed in the outer shells. Parts c and d of Figure 3 show calculations for these two cases. The restriction of the donor chromophores to the surface of the core leads to a loss of sensitivity to coronal swelling. On the other hand, the restriction of the trap chromophores to the core surface clearly improves the sensitivity of the method.

In finite geometries, the decay of $\langle G^s(t)\rangle$ strongly depends on edge effects. To obtain information on this dependence, we compare in Figure 4 the DD decay curves for chromophores randomly distributed throughout a filled sphere, for a cylinder with the same radius as the sphere but of infinite length, and for an infinite solution in the thermodynamic limit. The same chromophore density was used in all three calculations. The gradual loss of edge effects from sphere to cylinder to infinite solution causes an acceleration of the decay of $\langle G^s(t)\rangle$.

To this point, $u(r)$ has been described by a step function. Such a chromophore distribution will not always be found in real systems. For example, diblock copolymers have an interfacial region with a gradual change of polymer composition which affects the shape of the distribution of chromophores at A−B junctions. If we consider diblocks in which only the outer block is end-tagged, the chromophore distribution follows the radial distribution of the terminal polymer segments, which is not well described by a step function. Calculations for various geometries enable us to examine the sensitivity of $\langle G^s(t)\rangle$, and of the experimental techniques measuring $\langle G^s(t)\rangle$ to the form of $u(r)$.

We systematically calculated DD $\langle G^s(t)\rangle$ for several nonrandom model distributions in diblock copolymer spherical micelles using basic functions, *i.e.*, Gaussians and exponentials. In Figure 5 we compare $\langle G^s(t)\rangle$ for several nonrandom chromophore distributions in the coronae of spherical shells, where the maximum of the chromophore density was chosen to be either on the inner boundary of the shell (core−corona) or the outer boundary of the shell (corona−solvent). The latter situation could correspond to coronae made up of flexible chains which are end-tagged with the chromophore. If the chromophore has a favorable interaction with the solvent, the chromophores will be located near the corona−solvent boundary, but there will be a distribution of locations determined by the distribution of chain configurations. In contrast, if the chromophore has a strong attraction to the core and a strong repulsion from the solvent, the chromophores will be located near the core−corona boundary, but the distribution of chain conformations will result in a distribution of locations near the core. In the calculations, the total number of chromophores and the inner and outer radii were held constant. The corresponding distribution functions $u(r)$ are shown in the inset. Although there is a distribution of chromophore locations in both cases, having the distributions peak near the core vs near the solvent makes a dramatic difference in the decay of $\langle G^s(t)\rangle$. However, the decay curves for $u(r)$ modeled with a Gaussian function differ little from those corresponding to an exponential function. Therefore, it is not possible to determine fine details of the functional form of the distribution.

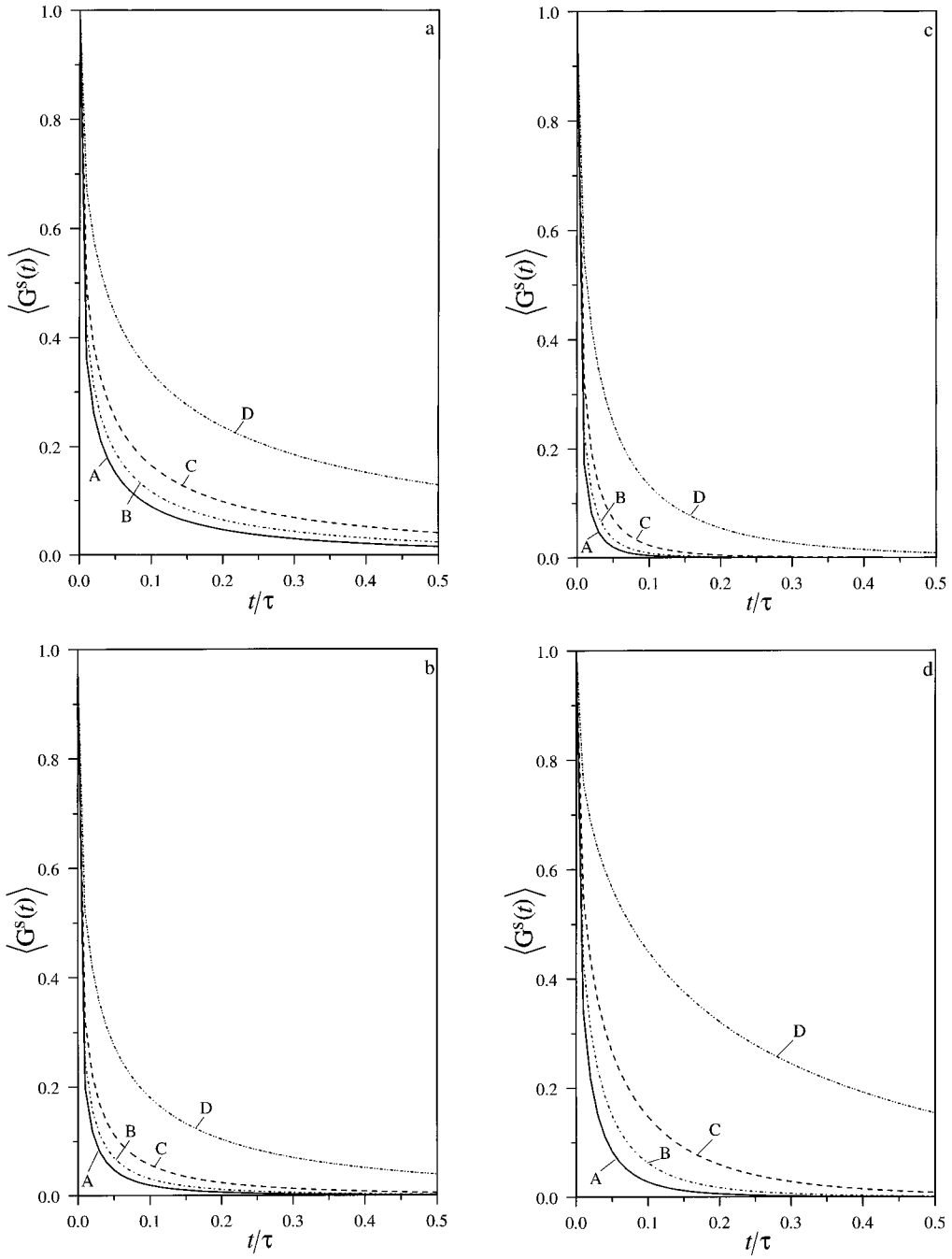

Figure 3. Effect of coronal swelling on $\langle G^s(t) \rangle$ in a micelle with $N = 30$, $R_{in} = 8$ Å, and $R_{out} = 16$ Å (curve A), 17 Å (B), 18.5 Å (C), and 23 Å (D): (a) donor−donor system in which all chromophores are randomly distributed in the coronae; (b) as in (a), but a donor−trap system (each micelle has a single donor and 29 traps); (c) as in (b), but donor chromophores are restricted to the surface of the core; (d) as in (b), but trap chromophores are restricted to the surface of the core.

Figure 6 shows calculations of DD $\langle G^s(t) \rangle$ for three symmetric distribution functions, a Gaussian, a double-sided exponential, and a rectangle. Each contains the same number of chromophores. These could represent chains that are tagged at the junction between the core block and the corona block in a diblock copolymer micelle. In such a system, the interfacial region is not sharp because of the distribution of chain conformations. From Figure 6 it is evident that the decay curves of $\langle G^s(t) \rangle$ are essentially indistinguishable. All of these distributions cover the same range of distances. If the distribution is expanded or contracted, the decays change. Therefore, it is possible to obtain information about the spatial extent of the interfacial region, but it is not possible to determine details of the functional form of the distribution. This is also the situation for DT systems.

IV. Conclusions

We have described the excitation transfer function $\langle G^s(t) \rangle$, the probability that the initially excited chromophore is still excited at time t, in a general way for both direct trapping in DT systems and for donor−donor transfer in DD systems. We have demonstrated the proper behavior of this model in those limiting cases for which analytical expressions in closed form are available. The general theory was applied to the special symmetries of spheres, shells, cylinders, and lamellae. These geometries were chosen because they span the tremendous architectural range of phases formed by diblock copolymers[1] and describe an abundance of natural forms assumed by lipid membranes and ciliated cells. More complex geometries can be studied by allowing the inner and outer radii of the shell to

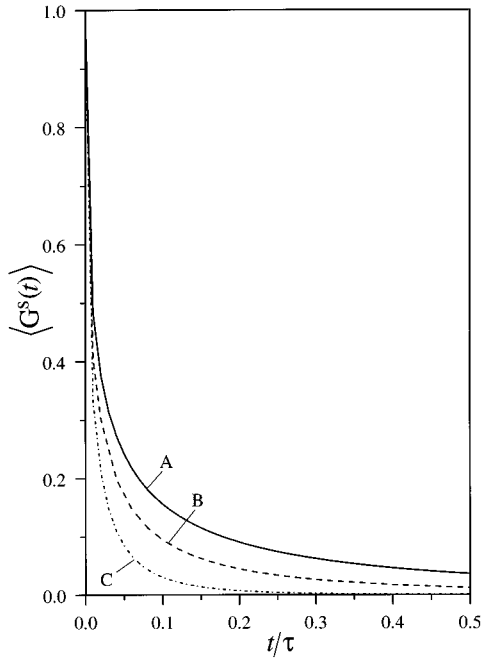

Figure 4. $\langle G^s(t) \rangle$ for a filled spherical volume with $N = 30$ and $R =$ 18.5 Å (curve A), an infinite cylinder with the same radius (curve B), and chromophores in the thermodynamic limit, randomly distributed in an infinite solution (curve C). $R_0 = 12.3$ Å, and the chromophore density is the same in all cases.

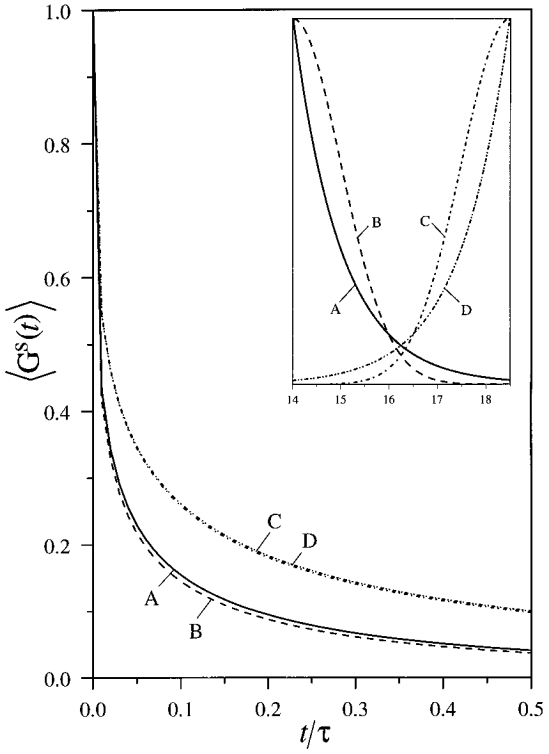

Figure 5. Effects of varying chromophore distribution in the corona on donor−donor $\langle G^s(t) \rangle$. $N = 30$, $R_{in} = 14$ Å, $R_{out} = 18.5$ Å, and $R_0 =$ 12.3 Å. Chromophores are packed close to the core surface for curves A (with density falling off exponentially into the solvent) and B (with density falling off as a Gaussian). Chromophores are packed close to the core−solvent interface for curves C (with exponential increase in density near the micelle surface) and D (with density increasing as a Gaussian). The chromophore distributions that give rise to the decays are shown in the inset.

vary with the angles θ and φ in spherical coordinates, which can be done in either a correlated or independent manner.

To investigate the sensitivity of $\langle G^s(t) \rangle$ to coronal swelling

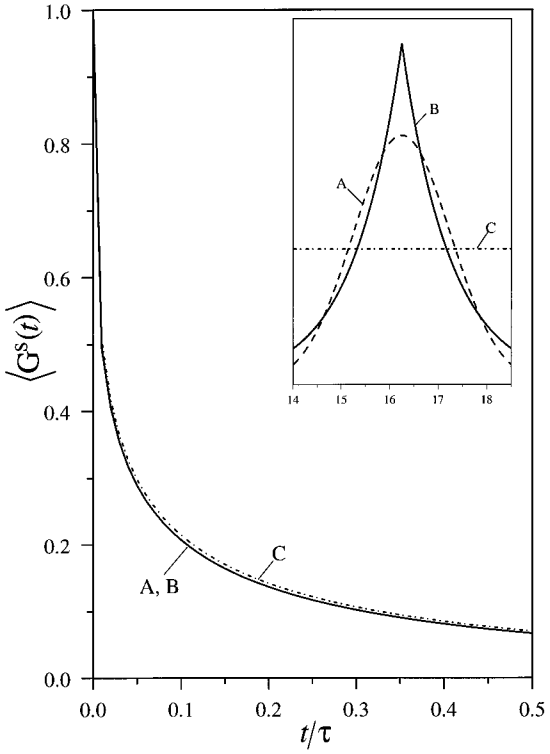

Figure 6. Effect on donor−donor $\langle G^s(t) \rangle$ of varying the shape of symmetrical chromophore distributions centered at the core−corona boundary located at 16.25 Å with $N = 30$ and $R_0 = 12.3$ Å. The inset shows the chromophore distributions corresponding to the decays: Gaussian (curve A), exponential (curve B), and rectangular (curve C). The curves show that it is not possible to determine the shapes of the distribution. However, the decays are sensitive to the width of the distribution.

such as that seen in diblock copolymer micelles, systematic model calculations were performed for DD and DT systems. We found that randomly labeling those blocks which will form coronae in a chosen solvent with donors is the preferred method for observation of this effect. The sensitivity can be enhanced by selectively tagging the junctions of the two blocks with trap chromophores.

Due to the general formulation of the theory for $\langle G^s(t) \rangle$ presented in this paper, introduction of any nonrandom chromophore distribution is straightforward. This allows us to investigate the sensitivity of $\langle G^s(t) \rangle$ to the shape of the chromophore distribution, which can be used to study the packing of chromophore-bearing polymer segments in the corona against the core of a micelle, their extension into a solvent, or the details of the chromophore distributions in the interfacial regions of diblock copolymer materials. We performed model calculations using several distribution functions and determined that details of the functional form of $u(r)$ in situations in which the chromophores occupy the same region are lost due to averaging over all chromophore positions in the calculation of $\langle G^s(t) \rangle$. However, configurational rearrangements that move chromophores from the core to the surface of a polymeric structure can be observed. We also find that the exact form of a symmetrical chromophore distribution at the A−B interface of a diblock copolymer system will not affect the observable appreciably; the observable is far more responsive to the thickness of the interface in both DD and DT systems.

Acknowledgment. This work was supported by the Department of Energy, Office of Basic Energy Sciences (Grant DE-FG03-84ER13251). The computers used in this work were provided by a departmental grant from the National Science

Foundation (Grant NSF-CHE-9408185). L.K. acknowledges support from the Holderbank Stiftung zur Förderung der wissenschaftlichen Fortbildung.

References and Notes

(1) Bates, F. S. *Science* **1991**, *251*, 898.
(2) Schmidt-Rohr, K.; Spiess, H. *Multidimensional Solid-State NMR and Polymers*; Academic: London, 1994.
(3) Förster, Th. *Ann. Phys (Leipzig)* **1948**, *2*, 55; *Z. Naturforsch. A.* **1949**, *4*, 321.
(4) Haan, S. W.; Zwanzig, R. *J. Chem. Phys.* **1978**, *68*, 1879.
(5) Gochanour, C. R.; Andersen, H. C.; Fayer, M. D. *J. Chem. Phys.* **1979**, *70*, 4254.
(6) Ediger, M. D.; Fayer, M. D. *Macromolecules* **1983**, *16*, 1839.
(7) Huber, D. L. *Phys. Rev. B* **1979**, *20*, 2307, 5333.
(8) Peterson, K. A.; Fayer, M. D. *J. Chem. Phys.* **1986**, *85*, 4702.
(9) Marcus, A. H.; Fayer, M. D. *J. Chem. Phys.* **1991**, *94*, 5622.
(10) Fredrickson, G. H.; Andersen, H. C.; Frank, C. W. *J. Polym. Sci.* **1985**, *23*, 591.
(11) Ediger, M. D.; Fayer, M. D. *J. Chem. Phys.* **1983**, *78*, 2518.
(12) Finger, K. U.; Marcus, A. H.; Fayer, M. D. *J. Chem. Phys.* **1994**, *100*, 271.
(13) Förster, Th. *Z. Elektrochem.* **1960**, *64*, 157.
(14) Baumann, J.; Fayer, M. D. *J. Chem. Phys.* **1986**, *85*, 4087.

JP953710D